S1. Source code of shallow water models

The source code of the advection models and the shallow water models using Double Fourier series (DFS) and spherical harminics (SH), which is written in Fortran, is included in the supplement. In the 'Source_code' folder, the files and folders below are included:

README.txt: README text file for the DFS and SH models.

LiCENSE.txt: Creative Commons Attribution-NonCommercial-ShareAlike 4.0 International License.

shallow_water_DFS: Folder for the DFS advection and shallow water models.

shallow_water_SH: Folder for the SH advection and shallow water models.

bihar: Folder for the Netlib BIHAR library.

The source code of the models is licensed under a Creative Commons Attribution-NonCommercial-ShareAlike 4.0 International (CC BY-NC-SA 4.0) license. These models utilize the Netlib BIHAR library and the ISPACK library. The Netlib BIHAR library is available at https://www.netlib.org/bihar/ and is also included in the Supplement. The ISPACK library is available at https://www.gfd-dennou.org/arch/ispack/ispack-3.0.1.tar.gz.

Please see REAME.txt to compile and execute the DFS and SH models.

S2. Conservation in shallow water test cases

We examined the conservation of mass, energy and vorticity in the Williamson test cases 1, 2, 5 and 6 (Williamson et al. 1992). We use the old DFS model with Grid [0], the new DFS models with Grid [0], Grid [1] and Grid [-1], and the SH model with the Gaussian grid. In the semi-Lagrangian atmospheric model using the old DFS method in Yoshimura and Matsumura (2005), a correction method (Priestley, 1993; Gravel and Staniforth, 1994) is used for global conservation of mass. In this study, however, we do not use the correction method for simplicity. To examine the conservation of mass and energy, we see the normalized difference of the global means between predicted values and initial values, which is normalized by the global mean of initial values. We see the global mean of vorticity as it is, since its exact value is zero.

Table S1 shows the results of the Williamson test case 1 in the Eulerian DFS and SH models with the truncation wavenumber $N \cong 2J^0/3$, where J^0 is the number of latitudinal grid points in Grid [0]. The normalized differences of the global means of mass between predicted values and initial values are very close to zero in all models at each resolution, which means that the conservation of mass is very good in the Eulerian models. Table S2 shows the same as Table S1 except that the semi-Lagrangian models are used and $N \cong J^0 - 1$. The conservation of mass in the semi-Lagrangian models are not so good as in the Eulerian models. We can improve this by using the correction method described above. The results are very similar between the models at each resolution. The conservation of mass becomes better as the resolution increases.

Tables S3, S4 and S6 shows the results in conservation for the Williamson test cases 2, 5 and 6, respectively. Table S5 is the same as Table S4 except that the truncation wavenumber is $N \cong 2J^0/3$ instead of $N \cong J^0 - 1$. The results are very similar between the models at each resolution. As the resolution increases, the conservation of mass and energy becomes better. The global means of vorticity is close to zero in all the models. The global means of vorticity in the DFS models using Grid [1] and Grid [-1] are not as close to zero as those in the DFS model using Grid [0] and the SH model. This seems to be because the accuracy of the meridional discrete cosine and sine transforms in the DFS models using Grid [1] and Grid [-1] is not as good as that in the DFS models using Grid [0].

Table S1. The normalized difference of the global means between the predicted values of mass (m) after a 12-day integration and initial values, which is normalized by the global mean of initial values. The results of Williamson test case 1 using the Eulerian models are shown. J^0 is the number of latitudinal grid points in Grid [0]. The truncation wavenumber $N \cong 2J^0/3$.

Resolution \ Model	Old DFS [0]	DFS [0]	DFS [1]	DFS [−1]	SH
J^0=64, N=42	Unstable	−5.6805E−14	−1.7060E−14	2.6562E−14	-6.3934E−14
J^0=160, N=106	Unstable	−2.0648E−13	−5.6674E−13	-7.8059E−13	-1.3305E−13
J^0=320, N=213	Unstable	−4.6783E−13	−2.4521E−12	-2.9143E−12	-3.0800E−13
J^0=960, N=639	Unstable	−3.8597E−13	−5.3336E−12	-5.0763E−12	-8.3133E−13

Table S2. Same as Table S2 except that the semi-Lagrangian models are used and the truncation wavenumber $N \cong J^0 - 1$.

Resolution \ Model	Old DFS [0]	DFS [0]	DFS [1]	DFS [−1]	SH
J^0=64, N=63	−9.4814E−2	−9.4807E−2	−9.4680E−2	−9.6345E-2	−9.2677E−2
J^0=160, N=159	−8.3514E−3	−8.3516E−3	−8.3519E−3	−8.3719E-3	−8.2474E−3
J^0=320, N=319	−7.0481E−4	−7.0483E−4	−7.0486E−4	−7.0551E-4	−6.9895E−4
J^0=960, N=959	−9.0290E−6	−9.0289E−6	−9.0287E−6	−9.0307E-6	−9.0467E−6

Table S3. The normalized difference of the global means of (a) mass, and (b) energy, between the predicted values after a 5-day integration and initial values. (c) The global mean of vorticity. The results of the Williamson test case 2 using the semi-implicit semi-Lagrangian models are shown. The truncation wavenumber $N \cong J^0 - 1$.

(a) Mass

Resolution \ Model	Old DFS [0]	DFS [0]	DFS [1]	DFS [−1]	SH
J^0=64, N=63	1.5703E−5	1.5702E−5	1.5700E−6	1.5610E−5	1.5488E−5
J^0=160, N=159	8.9819E−7	8.9819E−7	8.9822E−7	8.9728E−7	8.9248E−7
J^0=320, N=319	9.0058E−8	9.0059E−8	9.0055E−8	9.0025E−8	8.9722E−8
J^0=960, N=959	1.9977E−9	1.9977E−9	1.9973E−9	1.9969E−9	1.9946E−9

(b) Energy

Resolution \ Model	Old DFS [0]	DFS [0]	DFS [1]	DFS [−1]	SH
J^0=64, N=63	1.6165E−5	1.6164E−5	1.6173E−5	1.5921E−5	1.5917E−5
J^0=160, N=159	8.8305E−7	8.8305E−7	8.8303E−7	8.8039E−7	8.7620E−7
J^0=320, N=319	7.8240E−8	7.8242E−8	7.8235E−8	7.8149E−8	7.7842E−8
J^0=960, N=959	1.1127E−9	1.1127E−9	1.1122E−9	1.1112E−9	1.1096E−9

(c) Vorticity

Resolution \ Model	Old DFS [0]	DFS [0]	DFS [1]	DFS [−1]	SH
J^0=64, N=63	−1.1839E−23	−2.5849E−26	1.2169E−22	−2.1570E−22	1.3597E−23
J^0=160, N=159	6.2039E−25	4.3944E−24	−8.4567E−22	−8.3314E−22	−1.0340E−25
J^0=320, N=319	1.7732E−24	1.0934E−24	−2.6903E−21	−2.3009E−21	1.4760E−24
J^0=960, N=959	8.7500E−25	5.4493E−24	−3.1522E−21	−1.0864E−22	2.5324E−24

Table S4. Same as Table S3 except for the predicted values after a 15-day integration in the Williamson test case 5.

(a) Mass

Resolution \ Model	Old DFS [0]	DFS [0]	DFS [1]	DFS [−1]	SH
J^0=64, N=63	−6.0548E−6	−4.6793E−6	−4.5873E−6	−7.0440E−6	−4.5182E−6
J^0=160, N=159	2.4893E−6	2.5090E−6	2.5030E−6	4.1298E−6	2.5223E−6
J^0=320, N=319	1.7914E−6	1.7841E−6	1.7846E−6	1.5660E−6	1.7853E−6
J^0=960, N=959	5.2001E−7	5.2007E−7	5.2010E−7	5.2091E−7	5.2023E−7

(b) Energy

Resolution \ Model	Old DFS [0]	DFS [0]	DFS [1]	DFS [−1]	SH
J^0=64, N=63	−6.0548E−5	−2.2897E−5	−2.2626E−5	−2.6979E−5	−2.2042E−5
J^0=160, N=159	2.9058E−6	2.9450E−6	2.9361E−6	5.8088E−6	2.9842E−6
J^0=320, N=319	2.5944E−6	2.5825E−6	2.5831E−6	2.1968E−6	2.5866E−6
J^0=960, N=959	7.7936E−7	7.7949E−7	7.7952E−7	7.8096E−7	7.7986E−7

(c) Vorticity

Resolution \ Model	Old DFS [0]	DFS [0]	DFS [1]	DFS [−1]	SH
J^0=64, N=63	4.6322E−23	3.1433E−23	−6.6068E−22	7.2432E−22	1.3235E−23
J^0=160, N=159	8.4703E−23	5.5587E−23	−8.4448E−22	−1.1964E−21	−1.9588E−22
J^0=320, N=319	8.2056E−23	8.4703E−23	−8.7392E−21	2.4617E−21	−9.0659E−23
J^0=960, N=959	8.6689E−23	4.7976E−23	−8.8074E−21	−2.8945E−20	9.5953E−24

Table S5. Same as Table S4 except for $N \cong 2J^0/3$.

(a) Mass

Resolution \ Model	Old DFS [0]	DFS [0]	DFS [1]	DFS [−1]	SH
J^0=64, N=42	Unstable	−4.7404E−6	−4.7016E−6	−4.5291E−6	−4.6616E−6
J^0=160, N=106	Unstable	2.5200E−6	2.5208E−6	2.5297E−6	2.5216E−6
J^0=320, N=213	Unstable	1.7827E−6	1.7828E−6	1.7828E−6	1.7841E−6
J^0=960, N=639	Unstable	5.2029E−7	5.2031E−7	5.2031E−7	5.2030E−7

(b) Energy

Resolution \ Model	Old DFS [0]	DFS [0]	DFS [1]	DFS [−1]	SH
J^0=64, N=42	Unstable	−2.2433E−5	−2.2349E−5	−2.2042E−5	−2.2126E−5
J^0=160, N=106	Unstable	2.9846E−6	2.9866E−6	3.0023E−6	2.9950E−6
J^0=320, N=213	Unstable	2.5832E−6	2.5835E−6	2.5836E−6	2.5864E−6
J^0=960, N=639	Unstable	7.8001E−7	7.8003E−7	7.8003E−7	7.8001E−7

(c) Vorticity

Resolution \ Model	Old DFS [0]	DFS [0]	DFS [1]	DFS [−1]	SH
J^0=64, N=42	Unstable	−8.2718E−24	−6.5657E−22	−7.4950E−22	−1.4889E−22
J^0=160, N=106	Unstable	6.3527E−23	−5.8032E−21	−7.3163E−21	−9.7938E−23
J^0=320, N=213	Unstable	9.6615E−23	−3.9101E−21	−6.8080E−21	−1.1316E−22
J^0=960, N=639	Unstable	2.4485E−23	−2.0003E−20	−2.5579E−20	9.9262E−25

Table S6. Same as Table S4 except for the predicted values after a 14-day integration in the Williamson test case 6.

(a) Mass

Resolution \ Model	Old DFS [0]	DFS [0]	DFS [1]	DFS [−1]	SH
J^0=64, N=63	-3.1260E-4	-3.1248E-4	-3.1326E-4	-3.1499E-4	-3.1450E-4
J^0=160, N=159	-2.3077E-5	-2.3077E-5	-2.3362E-5	-2.3379E-5	-2.3101E-5
J^0=320, N=319	-5.1882E-6	-5.1882E-6	-5.2388E-6	-5.2341E-6	-5.1849E-6
J^0=960, N=959	-1.7562E-7	-1.7562E-7	-1.8092E-7	-1.8008E-7	-1.7562E-7

(b) Energy

Resolution \ Model	Old DFS [0]	DFS [0]	DFS [1]	DFS [−1]	SH
J^0=64, N=63	−9.8637E−4	−9.8618E−4	−1.0588E−3	−1.0378E−3	−9.8871E−4
J^0=160, N=159	−8.2136E−5	−8.2134E−5	−9.4349E−5	−9.1327E−5	−8.2147E−5
J^0=320, N=319	−2.0583E−5	−2.0583E−5	−2.3757E−5	−2.3198E−5	−2.0573E−5
J^0=960, N=959	−1.7466E−6	−1.7466E−6	−2.0565E−6	−2.0168E−6	−1.7465E−6

(c) Vorticity

Resolution \ Model	Old DFS [0]	DFS [0]	DFS [1]	DFS [−1]	SH
J^0=64, N=63	0.0E0	−1.5882E−22	−9.8066E−22	−5.4864E−21	0.0E0
J^0=160, N=159	1.6941E-22	−1.9058E−22	−2.1892E−20	−1.0916E−20	−1.6941E−22
J^0=320, N=319	1.5352E-22	4.2352E−23	−7.6428E−21	−5.8424E−20	−9.5291E−23
J^0=960, N=959	−1.5000E-22	−2.2940E−23	5.9142E−20	−1.4775E−19	−3.3528E−23

S3. Galewsky-like test case with north-south symmetric initial conditions

We ran the Galewsky-like test case using the north-south symmetric initial conditions created by adding the north-south opposite distribution of height and winds with perturbations in the southern and the northern hemisphere. Figure S1 shows the predicted vorticity after a 6-day integration in the Galewsky-like test case at 1.3 km resolution. The result in the new DFS model using Grid [0] is almost the same as that in the SH model. Figure S2 shows Kinetic energy spectrum of horizontal winds after a 6-day integration in the Galewsky-like test case. The results are almost the same for the DFS model and the SH model, but very small oscillations appear near the truncation wavenumber in the SH model. These results are similar to those in the Galewsky test case.

Reference

Gravel, S., and Staniforth, A.: A mass-conserving semi-Lagrangian scheme for the shallow-water equations, Mon. Weather Rev., 122, 243-248, doi.org/10.1175/1520-0493(1994)122<0243:AMCSLS>2.0.CO;2, 1994.

Priestley, A.: A quasi-conservative version of the semi-Lagrangian advection scheme, Mon. Weather Rev., 121, 621–629, doi:10.1175/1520-0493(1993)121<0621:AQCVOT>2.0.CO;2, 1993.

Williamson, D. L., Drake, J. B., Hack, J. J., Jacob, R., and Swarztrauber, P. N.: A standard test set for numerical approximations to the shallow water equations in spherical geometry, J. Comput. Phys., 102, 211–224, doi:10.1016/S0021-9991(05)80016-6, 1992.

Yoshimura, H. and Matsumura, T.: A two-time-level vertically conservative semi-Lagrangian semi-implicit double Fourier series AGCM, CAS/JSC WGNE Research Activities in Atmospheric and Ocean Modeling, 35, 3.25–3.26, 2005.

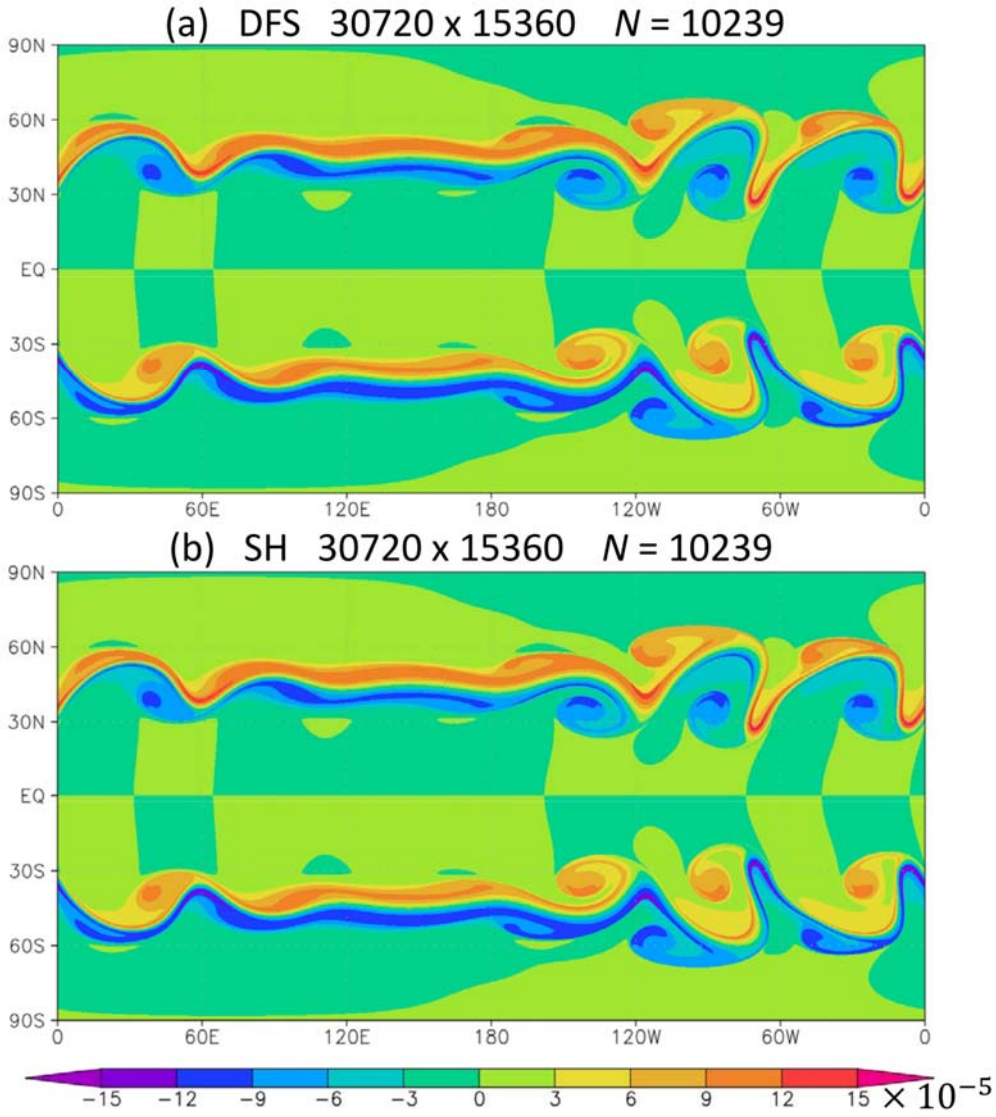

Fig. S1. Predicted vorticity (s^{-1}) after a 6-day integration in the Galewsky-like test case with north-south symmetry. (a) The new DFS model with Grid [0], and (b) the SH model at 1.3 km resolution with $I = 30720$, $J^0 = 15360$ and $N = 10239$.

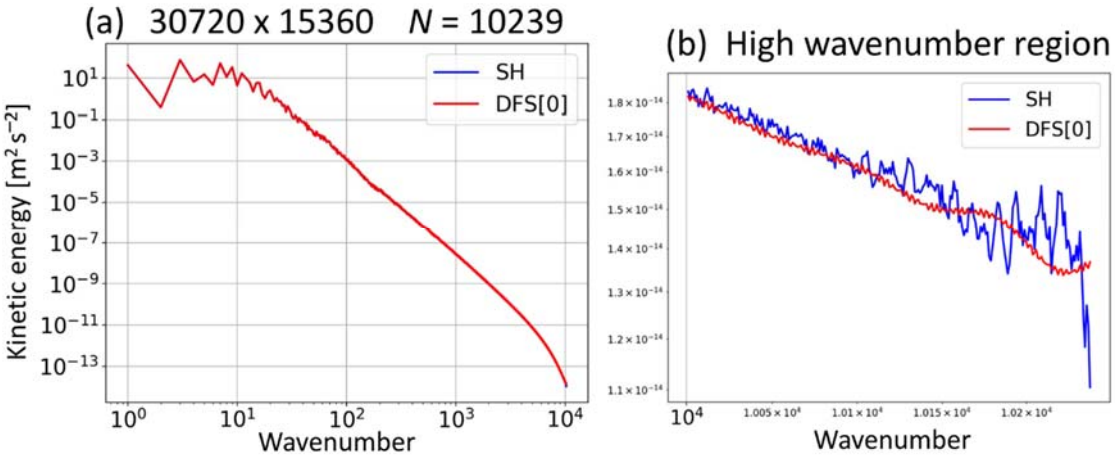

Fig. S2. Kinetic energy spectrum of horizontal winds ($m^2 s^{-2}$) after a 6-day integration in the Galewsky-like test case. (a) Results of the models with $I = 30720$, $J^0 = 15360$ and $N = 10239$. The colors blue and red represent the models using SH and DFS with Grid [0], respectively. (b) Same as (a), but showing the high-wavenumber region.